Wind Tunnel Modeling of Small Electric UAV Power System Performance

Nathan R. Phelps[1]
California Polytechnic State University, San Luis Obispo, California, 93410

This report details the design and construction of a testing apparatus for characterization of small electric aircraft power systems designed for use in the California Polytechnic State University San Luis Obispo Aerospace Engineering department's subsonic wind tunnel. This apparatus was constructed and implemented with the goal of determining system and component efficiencies of an entire power system using RC Aircraft components as an analog for systems currently in use in the current generation of small electric UAV's in service with the US Armed Forces. The goal of these experiments was to determine where improvements in the system architecture can be made with a specific goal of extending flight time beyond the current maximum of approximately two hours. It was found that for the test system, the biggest hindrance to optimal performance is the inverse relationship between motor and propeller efficiency. As motor efficiency is increasing, propeller efficiency decreases and the net effect is poor efficiency at all operating points. Additionally, it was found that input voltage has a large effect on overall motor and controller efficiency with a measured change in efficiency of 11% for a constant 10,000 RPM output at voltages ranging from 16.8 to 12 Volts. It was also found that further development is needed to make this apparatus an acceptable solution for precise characterization of actual UAV power systems. The current standard deviation in the power measurement of $\pm 28\%$ or $\pm 36.1\ W$ is much too large to provide any kind of accurate picture of the actual operating conditions.

Nomenclature

A	=	amps
C	=	dynamic pressure correction factor
D	=	diameter
P	=	pressure
ΔP	=	pressure differential
δP	=	output power standard deviation
L	=	length
mAh	=	milliamp hours
η	=	efficiency
P	=	pressure
ρ	=	density
q	=	dynamic pressure
R	=	gas constant
RC	=	remote control
RPM	=	revolutions per minute
UAV	=	unmanned aerial vehicle
V	=	voltage
W	=	watts

[1] Undergraduate Student, Aerospace Engineering, 1 Grand Ave, San Luis Obispo CA 93410, Student.

I. Introduction

Today's generation of small UAV enables members of the US Armed Forces to achieve a higher level of battlefield awareness than any previous generation of soldier. Products such as the AeroVironment Raven seen in Fig. 1 allow for real time imaging and position data to be relayed to a group of soldiers. This increase in battlefield awareness allows for soldiers to make superior tactical decisions and as a result the lives of the men and women who have dedicated themselves to protecting the people of the United States of America are protected with one more tool.

Figure 1 – A soldier launches an AeroVironment Raven Electric Unmanned Aerial Vehicle.

Although they provide a huge boost in battlefield awareness and increase overall soldier effectiveness, the current generation of small electric UAV systems is limited mainly by flight time. Current backpackable systems such as the Raven are limited to approximately two hours of flight time at the most, with the Raven itself achieving a maximum flight time of 90 minutes.[3] Increased performance could be achieved by lowering the weight of the non-functional components of the aircraft by use of lighter composite materials, or through an increase in power system efficiency or battery capacity. Reducing system weight by use of lighter structures is limited by the need for the aircraft to survive battlefield conditions. There is a minimum threshold on the acceptable durability of military UAV systems which limits the amount of material that can be removed to lighten the aircraft for flight characteristic improvements. In simple terms, the structural design of small UAV's is often determined by human handling concerns rather than flight loads. Because of these factors, this report looks to determine what kinds of improvements can be made in the design of the power systems used in these types of systems.

From current public research it is unclear whether current systems suffer most from low battery capacity, or from poor motor and propeller efficiency. By performing an analysis on the estimated in flight performance of each component of the power system, a recommendation can be made to focus research efforts in the future on the areas in which the aircraft are most in need of improvement. Due to the proprietary nature of the systems used in actual military UAV systems, in this iteration of the testing procedure, RC aircraft power system components will be used as an analog for the systems in use in actual UAVs. This allows for the testing system to be verified and for a baseline performance to be determined. RC Aircraft power systems represent a relatively advanced electric power system, with high output motor and controller systems and high energy density batteries being used to provide higher power, longer, more enjoyable flight for hobbyists. This is a less than perfect comparison, but it is hoped that with the system verified and valid results reported for the RC aircraft system, further research can be completed using the apparatus in conjunction with cooperation from a company such as AeroVironment or Aeromech to perform testing on actual UAV systems. It is felt that before asking such companies to sponsor the project with power system components it is necessary for the testing system to be validated.

II. Project Goals and Limitations

The primary goal of this project is to create a system which can fully characterize an electric power system of approximately 3-500W power output. Before asking for a company to sponsor future development of this project with actual UAV power system equipment, it is imperative that the system is proven and that it is shown that the data produced by the system is useful in characterizing a power system with reasonable margins of error. Performing tests on a remote control aircraft system is useful for purposes of proving the system works and provides meaningful insights into the performance of a battery, motor and controller and propeller system but this data is of

limited use as it is impossible to know in which areas and to what extent such a system differs from an actual UAV power system. It is highly likely that an actual UAV power system will have had much more extensive research put into proper matching of motor and propeller, battery capacity and operating voltage etc. but it is necessary to use such a poor representation at this point to prove the performance of the measurement system itself.

With this system, it is hoped that accurate measurements of propeller thrust, rpm, motor torque, current draw, and battery voltage can be recorded. With these metrics, the efficiencies of each individual component of the power system can be determined. With these values determined for various flight conditions, any general trends in the data can be analyzed to determine whether any one component is causing an undue amount of energy loss. At this stage in the development of this system, it is important to analyze the level of precision and accuracy the system achieves when taking these measurements. Once the precision and accuracy of the system has been verified, the verification power system will be characterized to both provide a baseline performance metric for future system tests and to also demonstrate the testing methods by which any power system donated by AeroVironment or another small electric UAV company will be characterized. In this way, a compelling argument for the donation of an expensive power system can be made.

The goal of the characterization process is to determine whether any single component is causing a significantly larger efficiency loss or if large efficiency losses are found throughout the system and the entire system from battery to motor to propeller is inefficient. If any one component stands out as significantly more inefficient, that component should be the focus of any further efforts to increase flight time as increased system efficiency will reduce the amount of energy required to keep the aircraft flying for a set period of time. With the energy draw reduced, the same amount of battery capacity can provide longer flight times. If no one component stands out as lossy, equal efforts should be put into better matching of components and increasing every component's efficiency to provide a meaningful combined efficiency boost.

One of the big unanswered questions regarding electric motor performance is the effect of battery voltage drop on the efficiency of a power system for a given power output. This is one of the main questions this project is looking to answer at this point. As motor design methods are relatively well known, it is felt that the motors are probably the component most closely related to those used in actual UAV systems. If battery voltage sag causes a large amount of efficiency loss, efforts should be put into creating battery chemistries that are able to maintain a more consistent voltage throughout the charge or into motor controller technologies that provide better performance over a wide input voltage range.

Propeller design is probably the weakest link in the use of RC aircraft power system components to model actual UAV components. Commercially available RC aircraft propellers are notoriously poorly designed as RC hobbyists are generally unable to measure propeller efficiencies and are in most cases able to overpower their aircraft and carry excess fuel (or battery capacity) to make up for any propeller design deficiencies. Unlike a UAV, most remote control aircraft do not need to carry a meaningful payload and thus can generally be overdesigned to the point that propeller efficiency becomes a nonissue. It is highly likely that the propellers being used on UAV's are much more well designed than those available for initial testing for this project. Because of this, any conclusion based on currently available propellers can only be used to make a tentative recommendation on further propeller development for actual UAV systems.

III. System Design and Construction

The foundation for this apparatus is the Cal Poly Aerospace Engineering Department's low speed wind tunnel. The windtunnel can be seen in Figure 2. The low speed windtunnel can provide up to approximately 80 mph freestream velocities and with a 3'x4" test section can test relatively large aircraft models or in this case, motor and propeller systems while still maintaining effective flow over the entire test apparatus without boundary layer interaction.

Figure 2 – Cal Poly Low Speed Windtunnel.

The most difficult aspect of apparatus design for this experiment was the combination of the need for torque measurement and clean airflow over the propeller for use in the wind tunnel. The former requirement would make a combined force/torque sensor ideal for the measurement of thrust and torque together in one sensor, but the currently available combined torque/force sensors are almost exclusively compression only sensors. To use such a sensor would require the sensor to be mounted upstream from the motor and propeller assembly, thus disturbing the airflow over the propeller and negatively affect the accuracy of the results. Because of this, an alternative solution was necessary.

After discussing design possibilities with this project's advisors Dr. John Dunning and Dr. Thomas Mackin, it was decided that a solution utilizing two tension load cells, one measuring thrust directly and one reacting torque through a lever arm was the best way to obtain the necessary physical data from the apparatus. The original hand sketch of this setup can be seen in Fig. 2. This apparatus consists of a linear bearing system mounted to a stand which positions the motor shaft at 1.5 ft from the base of the wind tunnel and directly in the center horizontally, placing the thrust centerline at exactly the center of the 3 ft high x 4 ft wide wind tunnel test section.

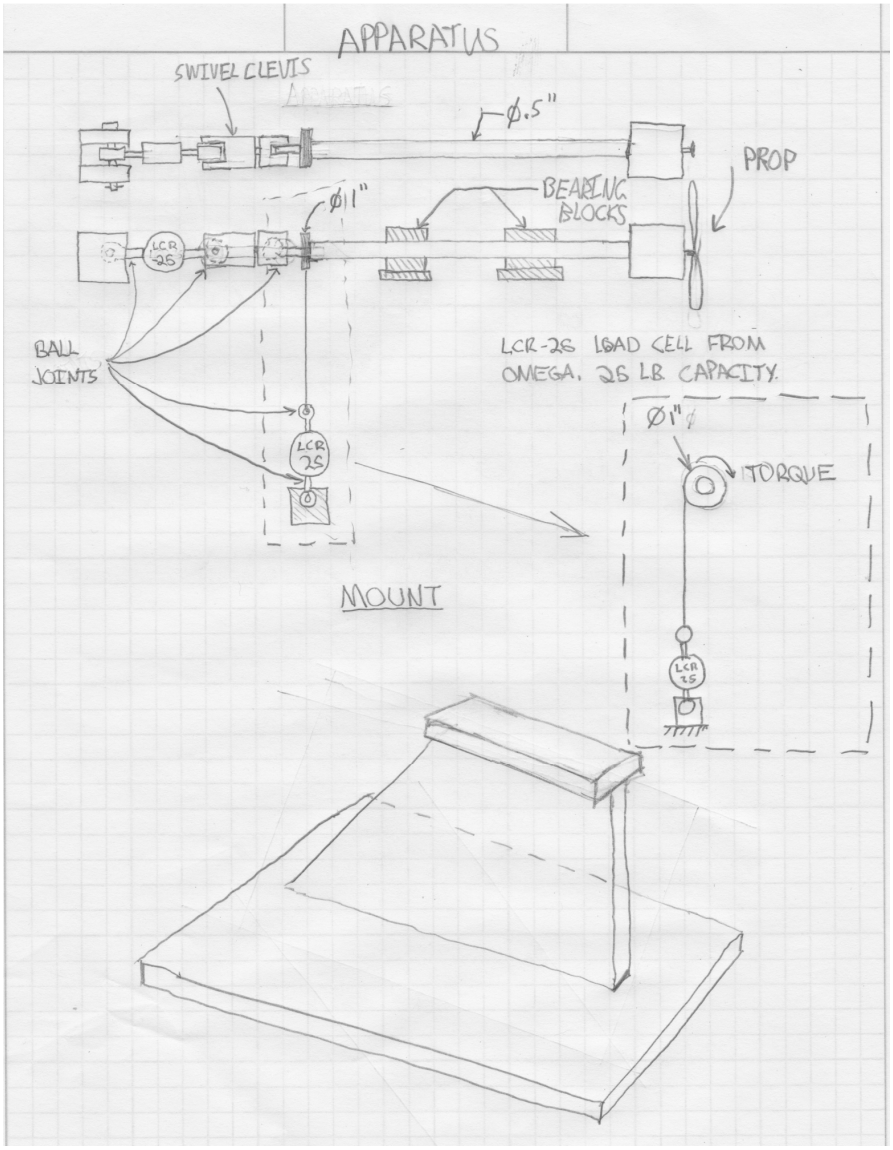

Figure 2 – Hand sketch of original apparatus concept.

The thrust and torque measurements are isolated by use of a bearing swivel which allows for the reaction torque arm and its corresponding load cell to freely react the motor's torque without interaction from the thrust measurement apparatus on the other side of the swivel. Every connection in the apparatus is done with Heim joint rod ends to prevent binding due to any misalignment.

This design went through multiple iterations, with the Omegadyne LCR-25 load cells specified by the original sketch being replaced by the Omegadyne LC703 load cell being the only significant change to the working apparatus. This was done to increase the precision of the measurements by utilizing a larger percentage of the load cell's usable range. The LCR-25 load cells are a 25 lb. rated load cell whereas the selected LC703 load cells are 10 lb. load cells. With an average thrust output of less than 5 lbs. of thrust for the power systems in this size range, utilizing 50% as opposed to 25% of the load cell's usable capacity results in superior precision while still providing a reasonable margin of safety. Additionally, the LC703 load cells are lower profile, allowing for the linear bearing blocks to be mounted farther apart, increasing the stability of the linear bearing system and reducing the probability that binding or other bearing system malfunctions will impact the accuracy of the system.

The torque sensing load cell takes its load from a 1" lever arm mounted to the back of the linear bearing system before the swivel. In this way the load cell's force output reading is actually in lb-in, the preferred torque measurement for motors of this size.

The design of the mounting system for the apparatus was determined by the existing wind tunnel apparatus. The wind tunnel test section has a 14”x21” mounting hatch directly forward of the sting balance apparatus. Because this testing apparatus is self-contained (that is, all measurements are taken with sensors built into the apparatus) using this hatch as the mounting point for the apparatus provided the simplest solution for securing the test system in the windtunnel.

The position of the motor and propeller in the windtunnel is crucial for optimized clean airflow. According to Dr. Jin Tso, who is responsible for everything windtunnel related in the Aerospace engineering department at Cal Poly, the boundary layer in the windtunnel has grown to a size which limits useful propeller diameter to approximately 12 inches. The propeller currently being tested is 9 inches in diameter, leaving a small margin of usable flow. Because of this, it is imperative to position the propeller directly in the center of the windtunnel to provide the cleanest airflow possible. To achieve this, the test apparatus must center the propeller horizontally and vertically, which results in a total height from the base of the apparatus to the centerline of the linear bearing, motor, and propeller apparatus of 1.5 feet.[5]

With these things in mind a basic design for the test stand was formulated and built from ¾” oak plywood. The plywood used was selected for its stiffness, surface finish and high ply count. With 11 plies, it exhibited excellent dimensional stability under varying environmental conditions and was the stiffest plywood available locally. Its veneer is a smooth, knot free oak which results in an ideal smooth surface to minimize the amount of airflow disturbance caused by the apparatus itself. The finished wood test stand can be seen in Fig. 3.

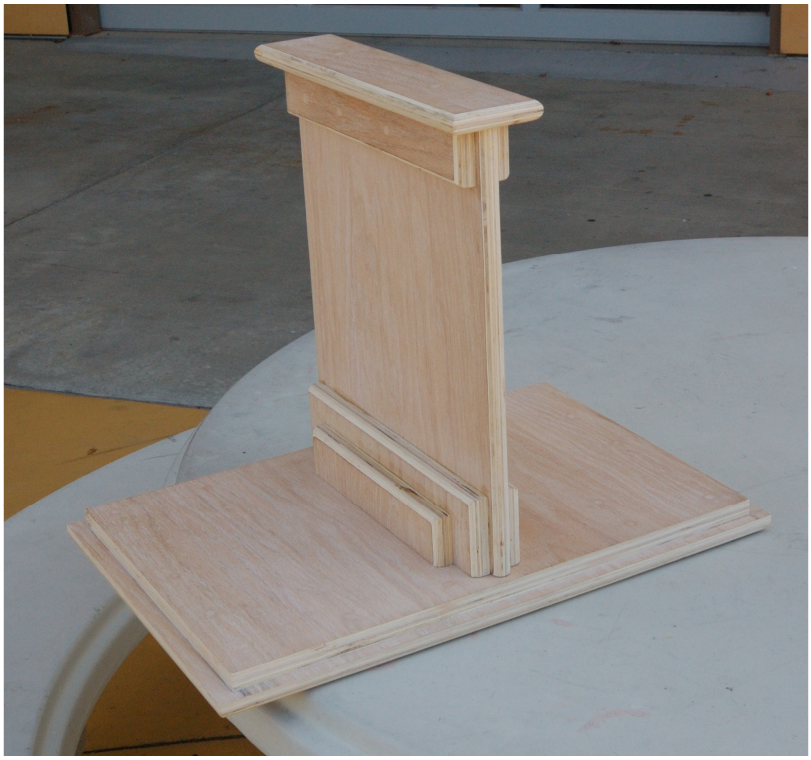

Figure 3 – Completed test stand base.

With the test stand base completed, the complete system could be assembled. The final layout can be seen in Fig. 4. And Fig 5.

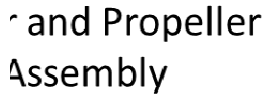

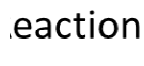

que load cells along with

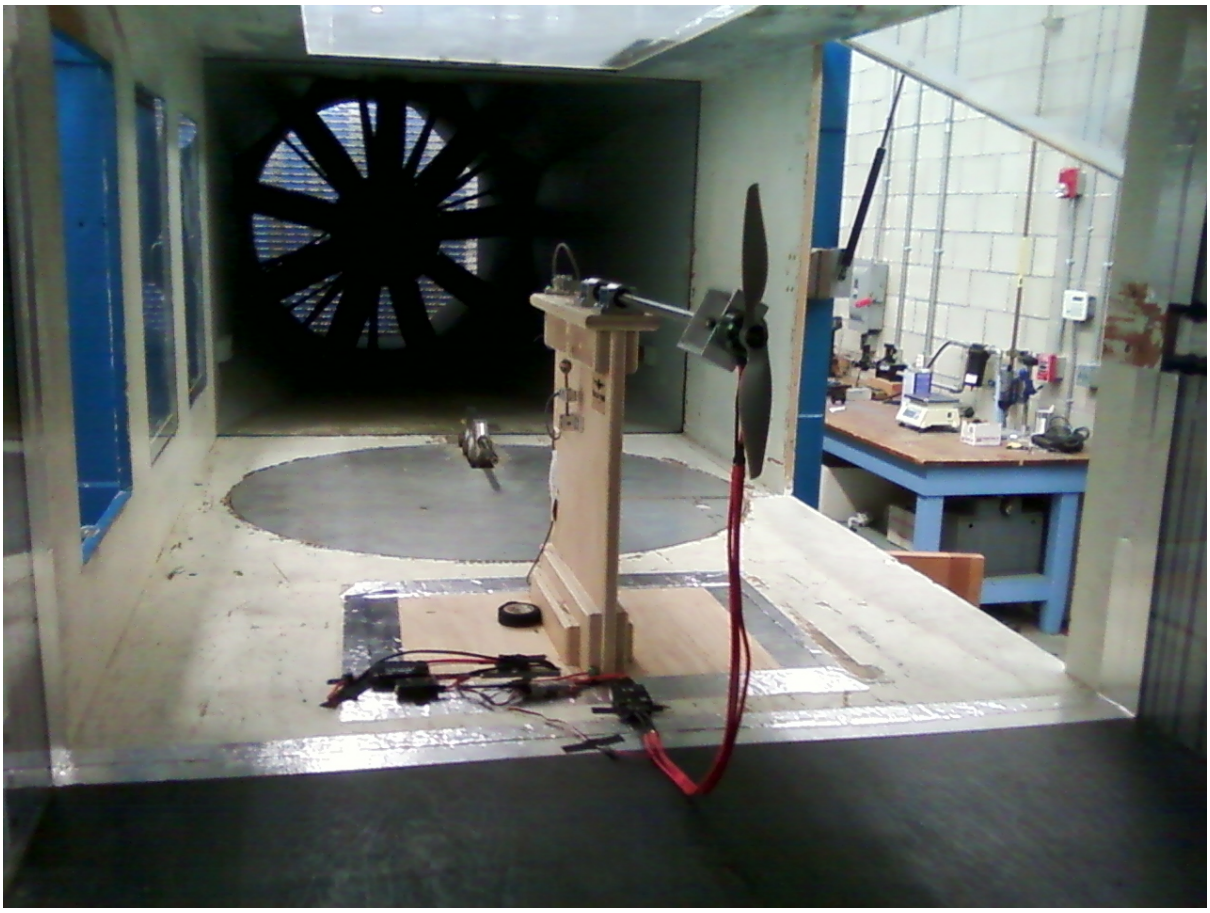

Figure 5 – Front view of apparatus installed in the windtunnel.

This assembly consists of the parts shown in Table 1.

Table 1 – List of parts used in apparatus.

Part	Description	Quantity
Thrust Load Cell	Omegadyne LC703-10	1
Torque Load Cell	Omegadyne LC703-10	1
Load cell ball joints	McMasterCarr P.N. 8928T11	4
Swivel Clevis	McMasterCarr P.N. 59915K271	1
Clevis Ball Joints	¼" Ball Joints Provided by Department	2
Linear Bearing Blocks	Thompson TSBP-8 ½" Pillow Block Ball Bearings	2
Linear Bearing Shaft	TQS1/2L-24 ½" Thompson Quick Shaft	1
Mounts and Torque Lever Arm	Custom Machined from 6061-T6 Aluminum	4
Tension Link	15 lb test braided fishing line	1
USB Data Acquisition	National Instruments USB-6211	1
Power Supply For Excitation Voltage	Cosel 12V switching power supply adjusted to 10V output	1
Motor Data Acquisition Card	EagleTree Systems V4 Datalogger	1

Thrust and motor torque data is collected via the Omegadyne LC703-10 tension link load cells and the National Instruments USB-6211 DAQ. The USB-6211 DAQ has 16 bit analog to digital converters, providing it with 65,536

quanta or divisions. The number quanta is equal to 2^n where n is equal to the number of bits used by the A/D converter.[10] From the National Instruments Spec sheet, it is found that the finest voltage range setting the USB-6211 is capable of is $\pm 200\ mV$.[11] Dividing this by 65,536 provides it with a theoretical ability to measure .0061 mV changes in input voltage. National Instruments specifies that the USB-6211 set to this sensitivity will accurately measure down to .088 mV changes in input voltage. This is greater than the value predicted by simply dividing the voltage range by the number of quanta available, but still provides sufficient resolution to accurately measure the thrust and torque values output by the load cells. With 10V excitation voltage, the load cells output approximately a $\pm 20\ mV$ maximum signal. This means that when measuring a 10 lb force (the maximum load the load cells are calibrated to measure), the DAQ will be able to accurately measure with a .44% margin of error. Even when measuring just 1 mV of input voltage from the load cells the USB-6211 will be able to measure with less than 10% margin of error. For the purposes of this experimental setup, this is more than satisfactory.

Thrust and Torque data from the DAQ is collected via a Labview virtual interface which saves the data to a csv spreadsheet file. This spreadsheet contains the load cell data along with a timestamp which records the time which the datapoint was taken down to the millisecond.

Motor RPM, current draw, and battery voltage are recorded by the EagleTree Systems V4 data logging system. This system consists of an IC which measures current and voltage by use of a small shunt and a sensor which detects the pulses from the motor controller to calculated motor RPM. This is the most accurate way of measuring motor RPM for synchronous brushless DC motors such as the motors expected for use in this apparatus. Because the motor RPM is exactly synchronized with the output of the controller, measuring these pulses provides an exact value for RPM while eliminating external sources of error that may exist when using optical or magnetic RPM sensors. Unfortunately, the data from the EagleTree Systems datalogger is output to a proprietary computer program which saves the data in a spreadsheet format. Because of this, the data from the EagleTree logger must be manually combined with the data taken in LabView. Because the experimental procedures in this lab only measure steady state values at an array of set conditions, this is not an issue as the systems can be run simultaneously and the outputs averaged and combined to obtain a full set of data points.

With the testing apparatus completed, the drive system could be installed. The basic drive system consists of the parts in Table 2.

Table 2 – Drive System Components.

Part	
Battery	GensACE 3300 mAh 25C rated 4S Lithium Polymer
Motor Controller	Hacker X-70 Opto Pro 3D
Motor	SunnySky 2814-8 1000 Kv Outrunner
Propeller	APC Thin Electric 9"x4.5"
Receiver	JR R770S PCM Receiver
Receiver Battery	JR 1100 mAh NiMH.
Transmitter	JR 6102 FM PCM Transmitter
Power Supply	BK Precision XLN3640

The Hacker motor controller and GensACE 3300 mAh battery were selected to provide ample headroom for the motor and propeller combinations to be tested. This battery can withstand up to 82.5 amps of continuous current and the controller can withstand 70 amps of continuous current. The SunnySky 2814-8 motor will be propped to pull approximately 34 A at full throttle, leaving a large margin of safety. Because this system is not being mounted in an aircraft, sizing the battery and controller with a large margin of safety decreases the likelihood that testing different propeller setups will damage the battery or controller. Use of this controller was decided after two smaller Castle Creations Phoenix 25 controllers were permanently destroyed after a particular motor and propeller setup drew twice the expected full throttle current. Catastrophic controller failure has the potential to damage other parts of the drive system and is also a fire hazard. The 70 amp maximum current of the Hacker controller allows for a much higher margin of safety than that provided by the 25 amp speed controllers being used originally.

The SunnySky 2814-8 motor represents a typical outrunner brushless motor used in today's RC aircraft. Outrunner brushless motors consist of a fixed inner stator assembly made up of thin iron plates with three sets of

copper wire windings surrounded by a rotating outer can containing high power rare earth magnets (in this case, neodymium magnets) as seen in Figure 6.

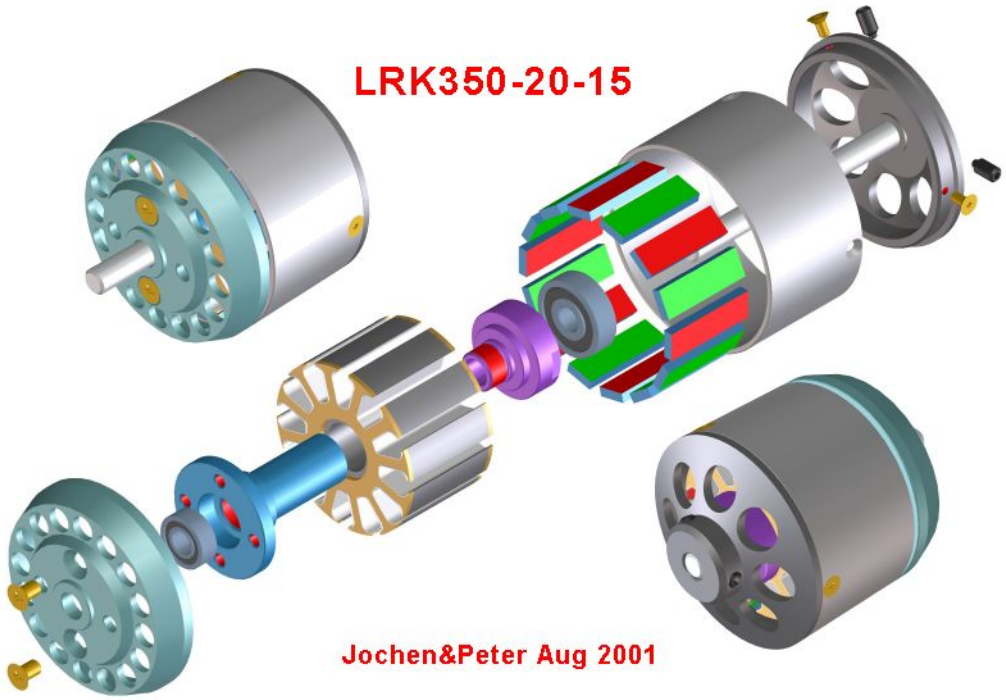

Figure 6 – Exploded view of a 12 pole stator, 14 magnetic pole outrunner motor design identical in configuration to that found in the SunnySky 2814-8. [7]

Outrunner brushless motors of this configuration operate in such a way that the electromagnetic fields created by the windings on the stator rotate seven times faster than the outer magnetic rotor and output shaft. In this way, outrunner motors contain an electromagnetic gear reduction, allowing them to efficiently turn large propellers without a mechanical gear reduction system. This is beneficial as it reduces complexity and also eliminates not only the efficiency losses of a gearbox but also the increased noise production characteristic of most gear drives.[6]

The GensACE battery will only be used to power the setup when metrics involving battery performance are desired. To eliminate unnecessary variables and complexity and to allow for testing to be performed without interruption for charging all testing for which battery performance is not a desired output will be performed with power being supplied by a BK Precision XLN3640 precision dc power supply. This power supply can output any desired voltage between 0-40 V and up to 40 A of current with a maximum power output of 1.44 kW. This is more than enough to supply the maximum draws expected from this motor. By setting a constant voltage output, tests performed to determine propeller performance will not be affected by changes in battery voltage output, allowing for higher repeatability and easier analysis.

Figure 7 shows the complete layout of the power system components.

IV. Technical Background and Procedure

Before taking any test data, it is necessary to verify the freestream velocity settings in the windtunnel. Freestream air velocity can be related to dynamic pressure, *q,* using Bernoulli's equation as in Eq. 1.

– (1)

Which can be related to the difference in the stagnation and static pressures in the wind tunnel as in Eq. 2.

(2)

For simplicity's sake, this pressure differential will be referred to for the remainder of the report as show in Eq. 3.

(3)

A function for the freestream velocity can be found by equating these two identities. This is shown in Eq. 4.

= – (4)

Which can be rewritten as shown in Eq. 5.

(5)

With this equation it is possible to accurately calculate the freestream velocity of the windtunnel using pressure measurements. Unfortunately, the only static pressure ports on the Cal Poly Aerospace Engineering Department's windtunnel are well upstream of the test location and as the boundary layer grows from its size at this point in the tunnel to its size at the test location the freestream velocity increases and with it the dynamic pressure. To correct for this, a series of data points is taken using a pitot-static probe installed in the test location. With the pitot-static probe installed, not only are the stagnation and static pressure values at provided by the built in pressure ports on the windtunnel known but the static and dynamic pressure values for the test location can be found as well. Using these values and a series of velocities, a correction factor can be found to predict dynamic pressure and therefore velocity at the test section using the built in pressure ports only. This correction factor is shown in Eq. 6.

$$C = \frac{q_{test\ section}}{q_{tunnel\ ports}} \tag{6}$$

And remembering that q is equal to ΔP

$$C = \frac{\Delta P_{test\ section}}{\Delta P_{tunnel\ ports}}$$

Using this value, an equation for test section velocity can be found. Equation 7 shows this calculation.

$$V = \sqrt{\frac{2C}{\rho}}\sqrt{\Delta P_{tunnel\ ports}} \tag{8}$$

Because $\Delta P_{tunnel\ ports}$ is measured in in-H_2O and the velocity calculation requires this measurement to be pounds per square foot, it is necessary to include a unit conversion factor into this equation. This correction factor is equal to

$$1\ in - H_2O = 5.2023\ \text{psf} \tag{9}$$

Which input into the velocity calculation results in Eq. 10; the final calculation for velocity used in this report.

$$V = \sqrt{\frac{5.2023 * 2C}{\rho}}\sqrt{\Delta P_{tunnel\ ports}} \tag{10}$$

This corrected value represents the best combination of calculation ease and accuracy for practical wind tunnel usage. The density value used in this equation is found from measured atmospheric data. At the time of the test as shown in Eq. 11.

$$\rho = \frac{P}{RT} \tag{11}$$

This correction procedure is outlined in more detail in *Low Speed Wind Tunnel Testing* by Barlow, Rae, and Pope.[1]

With the windtunnel calibrated, the load cells on the apparatus itself must be calibrated. This is done using standard weights to put a range of known forces on the load cell to allow for a calibration curve to be developed. Omegadyne supplies calibration data for their load cells, but this data does not take into account any effects the apparatus may have on the measurements. Calibrating with the load cells mounted in the test apparatus ensures that the applied forces are accurately recorded.

To calibrate the thrust load cell, loads from .5 to 4 lb were suspended from a pulley system which places a direct axial tension load on the apparatus. The millivolt output of the load cells was recorded for each of these measurements and a linear line of best fit was found using Excel's built in line fitting algorithm.

The torque load cell was calibrated in a similar manner, with the only difference being the calibration was done to match load cell voltage output to applied torque instead of axial force.

The test procedure itself consists of three tests. The first will determine the effects of battery voltage drop on the efficiency and power output of the system under constant throttle input. A throttle input of approximately 75% was chosen to provide adequate power output to excite the load cells while not overtaxing the power system, which will

be left in this condition for the entire duration of the test procedure. The battery will begin fully charged and will be allowed to discharge naturally as the test progresses. As the battery discharges, the power output of the system will be allowed to drop naturally. Data collection is done by taking sets of point data for approximately 15 seconds at intervals of 30 seconds between each data acquisition period. Once the data is collected, the first step is to calculate output power in horsepower as shown in Eq. 12.[2]

$$Power_{hp} = \frac{RPM*2\pi*T}{396000} \tag{12}$$

Where T is measured in lb-in. This number must then be converted to watts, the preferred unit of power for electric motors. For the purposes of this report, the conversion from horsepower to Watts will be done using the standard Metric system identity

$$1\ hp = 735.5\ W \tag{13}$$

This is done as shown in Eq. 14.

$$Power_{out_W} = P_{hp} * 735.5 \tag{14}$$

And from this a direct calculation for $P_{motor\ out_W}$ can be calculated

$$Power_{motor\ out_W} = \frac{735.5\pi*RPM*T}{198000} \tag{15}$$

To calculate motor efficiency, this value is compared to the input power which is simply calculated from measured data as shown in Eq. 16

$$Power_{motor\ in} = V * A \tag{16}$$

Efficiency is defined as

$$\eta_{motor} = 100 * \frac{Power_{motor\ out_W}}{Power_{in}} \tag{17}$$

These calculations were taken from a user manual supplied by Aveox, the motor manufacturer for the Raven UAV system.[9]

With this calculation completed for a set of operating points from fully charged to empty, a first look into the effects of battery voltage drop on motor and controller efficiency and power output can be evaluated. This information can be used to help determine whether research into battery technology that does not experience such a drastic change in voltage from fully charged to empty or motor controller technology that is less effected by battery voltage loss would be beneficial and to what degree. This concludes the testing that requires the battery as the power source. This test can also be run without use of the windtunnel if necessary, but the airflow isolation provided by the windtunnel ensures the results are not skewed by any changes in conditions that may be present during a test run in a normal room.

The second test serves to provide a better controlled evaluation of the effects of battery voltage on the efficiency of an electric power system. When using a battery as the power source, it is nearly impossible to maintain a constant power output. Continual throttle position adjustment is needed to maintain a constant thrust setting. As the battery voltage drops, the throttle position corresponding to a certain output power is continually changing. This makes accurate measurements difficult, as comparing motor efficiency accurately requires that the output power of the motor remains relatively constant. Comparing efficiency values for different output power levels is of limited use as motor and propeller efficiency are both dependent on operating condition.

For this test, the Gens ACE battery is replaced by the BK Precision XLM3640 precision DC power supply as the voltage source. In this way an input voltage can be set and held constant while the output RPM value is set. By setting the output RPM to the same level for each test, the output power will be approximately equal with only the input power varying. With the power supply connected test runs are performed at three voltage levels corresponding to peak, nominal, and minimum voltage levels for the battery pack being modeled. In this test, these voltage levels were those corresponding to a four cells in series configuration pack (The configuration of the GensACE 3300 mAh

pack used in the previous test). Fully charged voltage, nominal voltage, and minimum voltage were set at 16.8V, 14.8V, and 12 V respectively. These voltages correspond to 4.2 V/cell, 3.7 V/cell and 3 V/cell. At each power supply output voltage setting data points were taken at 12,000 and 10,000 rpm settings.

The third test is designed to fully characterize the propeller and motor combination over a range of in-flight operating points. This is done by running sweeps of power settings and test freestream velocities. To simplify testing and allow for extended run times, these tests will also be performed with the BK Precision XLM3640 power supply. Input voltage will be set at a nominal value representing the corresponding average pack voltage.

With data collected on the thrust, RPM, torque, motor amp draw, and battery pack voltage the motor and controller system and the propeller can both be fully characterized. Motor input and output power are defined in the same way used by the first experimental procedure. Propeller input power is equal to motor output power. The propeller output power is defined as

$$Power_{Prop\ Out} = Thrust * Velocity \tag{18}$$

This equation was taken from basic power calculations as outlined in *Fundamentals of Physics*.[4] In this case, thrust is measured in lbs and velocity is measured in ft/s so power in this equation is measured in lb*ft/s. To convert this to power in Watts requires multiplying by 1.356, therefore propeller power out in watts is equal to

$$Power_{Prop\ Out_W} = 1.356 * Thrust * Velocity \tag{19}$$

With this value found, propeller efficiency can be calculated as

$$\eta_{prop} = 100 \frac{Power_{Prop\ Out_W}}{Power_{Prop\ In_W}} \tag{20}$$

Where

$$P_{Prop\ In_W} = Power_{motor\ out_W} \tag{21}$$

This is the same relationship used by the motor efficiency calculation as provided by the Aveox manual.[9]

With these metrics, the power system can be fully characterized to any desired level of precision based on needed accuracy and time available. For the purposes of this project, initial testing will be carried out by sweeping velocity in 7 mph (10.26 ft/s) steps starting at 0 mph and ending at 42 mph (61.6 ft/s) and sweeping power settings in 20% increments from 20% power to 100% power. In this way a mesh of data points can be assembled which represent the performance of a particular motor and propeller combination with a particular input voltage under any freestream flight velocity or motor power setting inside of the measurement range.

Because all of the data used in this experiment is point data, data reduction was done using a simple average for each data condition. Use of an exponentially weighted moving average or other data smoothing procedure provides no benefits when the only parameters being analyzed are steady state conditions. If it were desirable to allow for the system to record data when conditions were changing use of such algorithms would prove beneficial.

V. Results and Discussion

Before running the tests, measured atmospheric data was recorded and the air density was calculated based on this data to allow accurate setting of the windtunnel speed. This data is shown in Table 3.

Table 3 – Atmospheric Data Recorded At Time of Test Runs

Property	Value
Temperature (F)	**60.2**
Atmospheric Pressure (in-Hg)	**30.1**
Density (slug/ft^3) (Calculated)	**.002387**

Using this data and Eq. 8 the dynamic pressure values for each test condition were calculated. For this test, the correction factor *C* was taken from calibration data recorded by Aerospace Engineering graduate student Jarred Pinn at the same test location. This data was taken earlier this quarter under the exact test conditions used for this experiment and resulted in a *C* value of 1.0832. The final equation used to determine test section velocity using this correction factor value and the atmospheric conditions at the time of the test is shown in Eq. 22.

$$Velocity = 68.8434\sqrt{\Delta P} \tag{22}$$

The calculated values for the third test procedure run conditions using this data are shown in Table 4.

Table 4 – Test Velocities and Dynamic Pressure Settings

Test Velocity (mph)	Test Velocity (ft/s)	Dynamic Pressure (in-H_2O)
7	10.26	.0222
14	20.53	.0889
21	30.8	.2002
28	41.06	.3557
35	51.3	.556
42	61.6	.8006

With this data compiled, the test apparatus was installed and calibrated. The final calibration curve for the thrust load cell is shown in Fig. 8. This data shows good linearity and an excellent fit with an R^2 value of .9961.

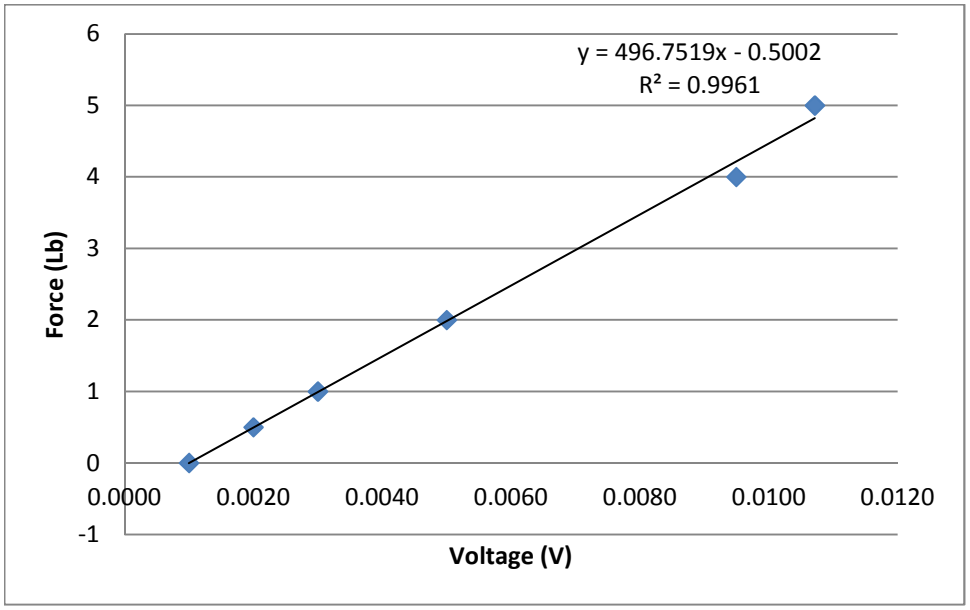

Figure 8 – Thrust load cell calibration.

Calibration of the torque load cell proved more challenging. From a few initial calculations it was found that the original calibration values shown in Fig. 9 were producing torque values that were unreasonable. Using these torque values the calculations outlined in the procedure section produced motor efficiencies of over 100%, which is a physical impossibility.

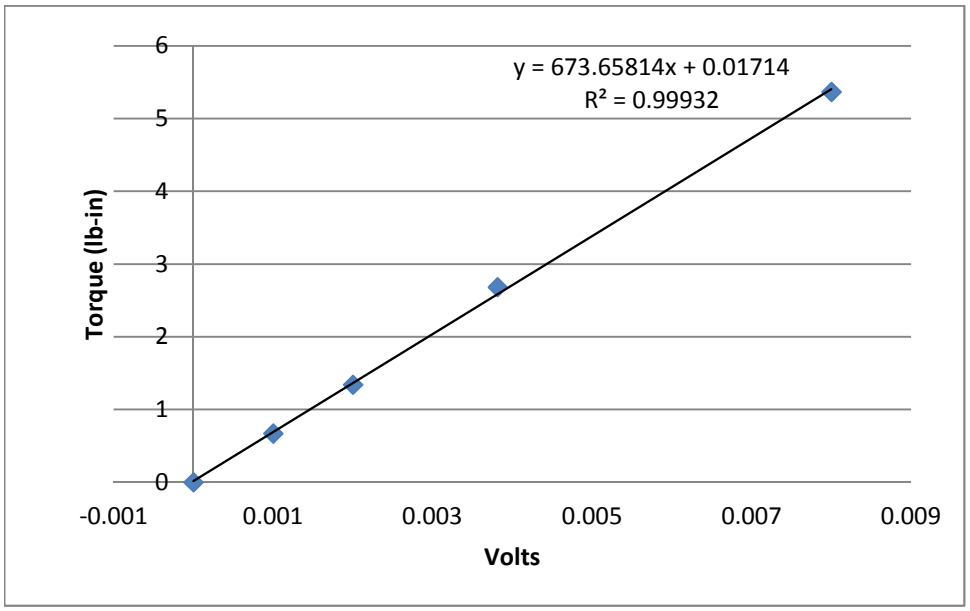

Figure 9 – Original Torque Calibration Curve.

After more analysis of the calibration data, it was found that two issues were affecting the accuracy of the torque calibration. The first, stiction in the linear bearing system, was causing the torque applied to the load cell to be systematically lower than that applied at the motor mount. Under static conditions (Such as those present during calibration) the linear bearings themselves were reacting a certain percentage of the applied torque. Under test conditions, the oscillations in the motor output RPM and therefore torque combined with the vibration caused by the operation of the combined motor and propeller system allowed for this stiction to work its way down to a value much closer to the actual value.

The second issue was that under operation, there is a small amount of measured torque output even when the motor is running in a no load condition. This torque output is a power loss – it represents the torque needed to overcome the friction in the motor bearings as well as the torque needed to overcome the aerodynamic forces generated by the fanlike characteristics of the motor's outer casing (Motors of this type are often designed with this characteristic as a feature to improve motor cooling). This torque is not output to the propeller and if left in the measurement is a source of error.

To combat these two issues, three things were done to improve the calibration accuracy. First, calibration was performed with the motor running at a constant 11,000 RPM. This represents a median RPM value at which an estimated value of the no load torque could be included into the calibration data. In other words, a built in calibration offset. This was done because it proved exceedingly difficult to collect accurate data for the motor's no load torque value with this system. The magnitude of this torque is very small and when attempting to establish the no load torque output of the motor at various run conditions it was found that the measured values did not follow any general trend and were instead quite random, with all values above ~10,000 RPM clustering in one general area. Because of this, it was decided to include this measurement with the calibration of the system instead of subtracting it out in post processing. Running the motor during calibration also provided a vibration which can help to reduce the effects of stiction on the accuracy of the measurements.

The second calibration improvement was lengthening the lever arm used for calibration from 1" to 2". By doing this, the magnitude of the calibration moments was increased, decreasing the relative effects of stiction on the system. 2" was chosen as it allowed for the largest 4 lb calibration mass to be used while still remaining well within the 10 lb force limit of the load cell (Approximately 8 lb force as seen by the load cell).

Lastly, a bracketing procedure was used to obtain an average calibration value that best represented the actual torque output of the system. First, calibration data was taken by placing the load onto the apparatus as gently as possible, allowing each mass to settle naturally as the system responded to its weight. With all of these data points taken, another set of datapoints was taken by placing the calibration weights and then gently pulling down on the weight and releasing before collecting data. In this way, the effects of stiction are accounted for from both directions and the average value will represent the true average value of the torque output. The final calibration curve for the torque load cell can be seen in Fig. 10.

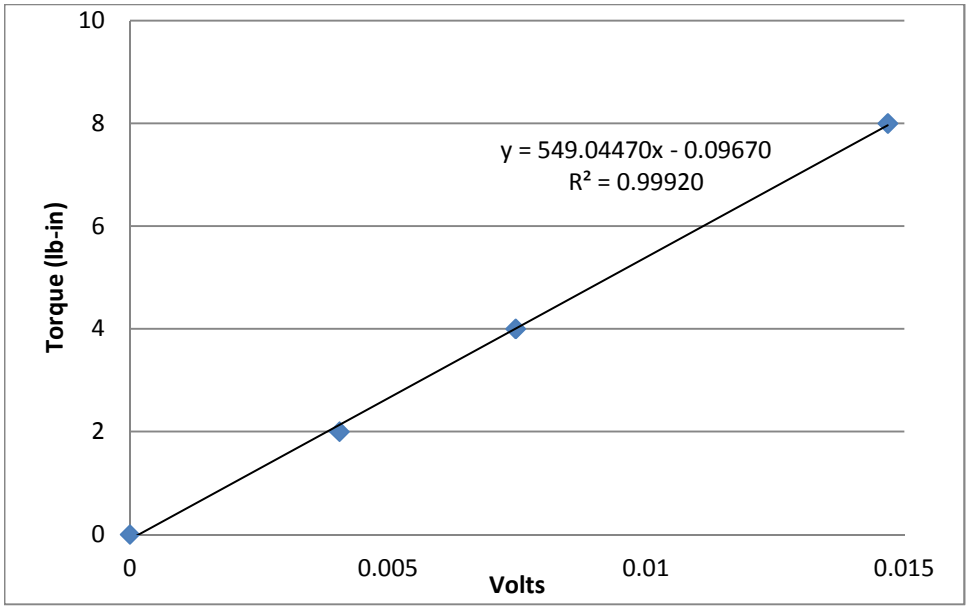

Figure 10 – Final Torque Calibration Curve. Notice the much smaller multiplier present in the fitted equation.

Final calibration data for both load cells can be seen in Table 5.

Table 5 – Calibration Data for Thrust and Torque Load cells

Thrust		Torque	
Voltage	Force (lb)	Voltage	Torque (lb-in)
0.00100	0	0	0
0.00200	0.5	0.004057	2
0.00300	1	0.00747	4
0.00500	2	0.014677	8
0.009493	4		
0.010712	5		

With calibration completed, the testing procedures could begin. It is important to note that for the purposes of this experiment, the motor and controller are analyzed as one unit. Measuring the values of the 3 phase AC output of the motor and controller is too complex for the purposes of this experiment. Some of the gains attributed to the motor itself in this experiment may be due to varying operating efficiency of the motor controller itself. As voltage drops the duty cycle of the motor controller at the same output power increases which can have an effect on the system's efficiency as a whole. This is acceptable for the purposes of this experiment as the controller efficiency is an integral part of the operation of any electric power system. It is impossible to operate a brushless AC motor such as the SunnySky 2814-8 without a motor controller so the inclusion of controller efficiency does not degrade the validity of the conclusions drawn from the data. For simplicity's sake for the rest of the report the combined motor and controller efficiency will simply be called motor efficiency.

As outlined in the procedure section, the test procedures started with running at a constant power setting using the Gens ACE 3300 mAh 4S1P battery pack and allowing the battery to discharge while taking data points at 45 second intervals. The compiled data for this test can be seen in Table 6.

Table 6 – Constant Throttle Setting Run with Gens ACE 3300 mAh 25C 4S1P Battery.

Torque (Lb-in)	Thrust (Lb)	Voltage (V)	Current (A)	RPM	Power in (W)	Power Out (W)	Motor Efficiency (%)
2.51	3.71	15.89	29.78	13418.93	473.14	392.66	82.99
2.42	3.57	15.35	29.08	13166.05	446.54	372.29	83.37
2.39	3.54	15.02	29.16	13094.71	437.99	365.49	83.45
2.35	3.48	14.82	28.78	13009.91	426.53	356.78	83.65
2.35	3.48	14.82	28.78	13009.91	426.53	356.34	83.54
2.33	3.45	14.59	28.64	12942.65	417.82	352.02	84.25
2.07	3.00	13.56	25.86	12247.39	350.50	295.19	84.22

The first thing to notice from this data is that the efficiency of the motor does not vary with voltage to any great degree. The maximum difference in efficiency values is 1.23%, which although measurable is not a large enough difference to drive selection of motor and battery setups. Motor efficiency is plotted against battery voltage in Fig. 11.

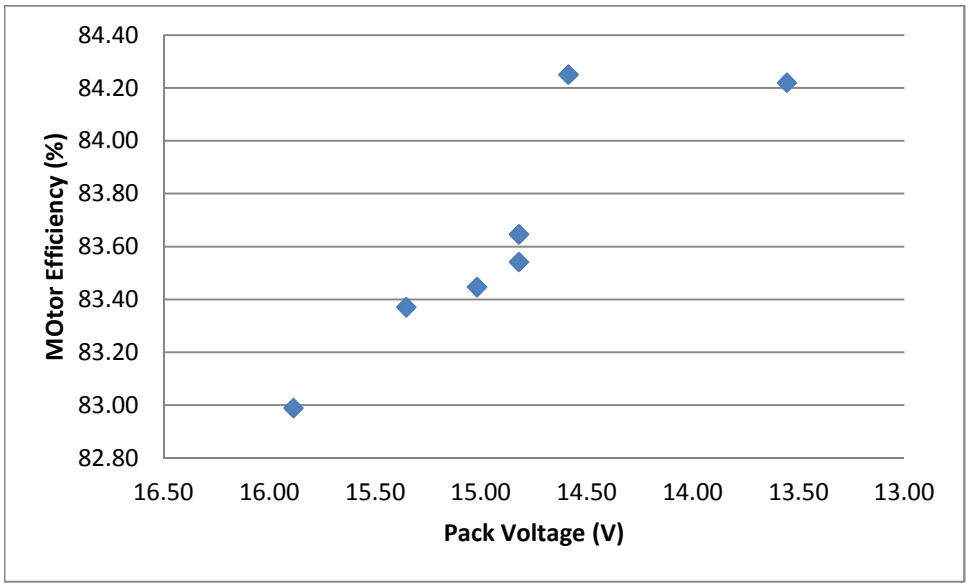

Figure 11 – Motor efficiency plotted against pack voltage.

It may seem as if there is a downward trend in efficiency as input voltage increases. This conclusion cannot be made at this point, because as seen in Figure 12 below, the power in and power out of the system are both dropping as the battery voltage drops. Without holding these values constant, any conclusions about the effects of battery voltage on motor efficiency are tenuous at best.

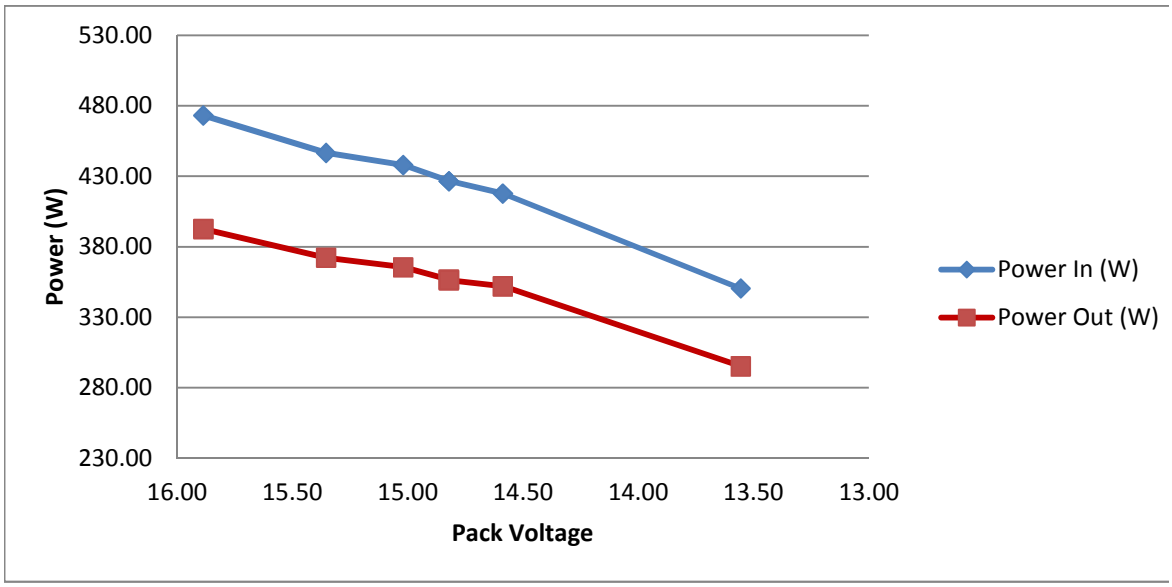

Figure 12 – Power in and out of the motor as battery voltage decreases at a constant throttle setting.

Figure 13 shows that the pack current and motor RPM both follow the same general trend as the power out, decreasing as the voltage decreases at a proportional rate. This data conclusively shows that a constant throttle setting test is useful for gaining insights into the behavior of the system under use, but is of limited use when looking to characterize the system as the varying voltages and corresponding current draw, output RPM and power values do not allow for direct evaluation of the effects of one parameter change. To perform this type of analysis with a battery powered system, it would be necessary to either develop a system which can manually hold the RPM value at the same point to a high degree of accuracy or use a motor controller that has a governor setting which attempts to hold the motor RPM constant over the entire discharge cycle. Motor controller algorithms of this type are most often found on motor controllers designed specifically for use in helicopters, where maintaining a constant head speed (output RPM at the rotor) is crucial for maintaining consistent flight properties. If in the future analysis of motor and propeller performance using a battery as the power supply is a desired experiment it is suggested that a controller with this capability is used.

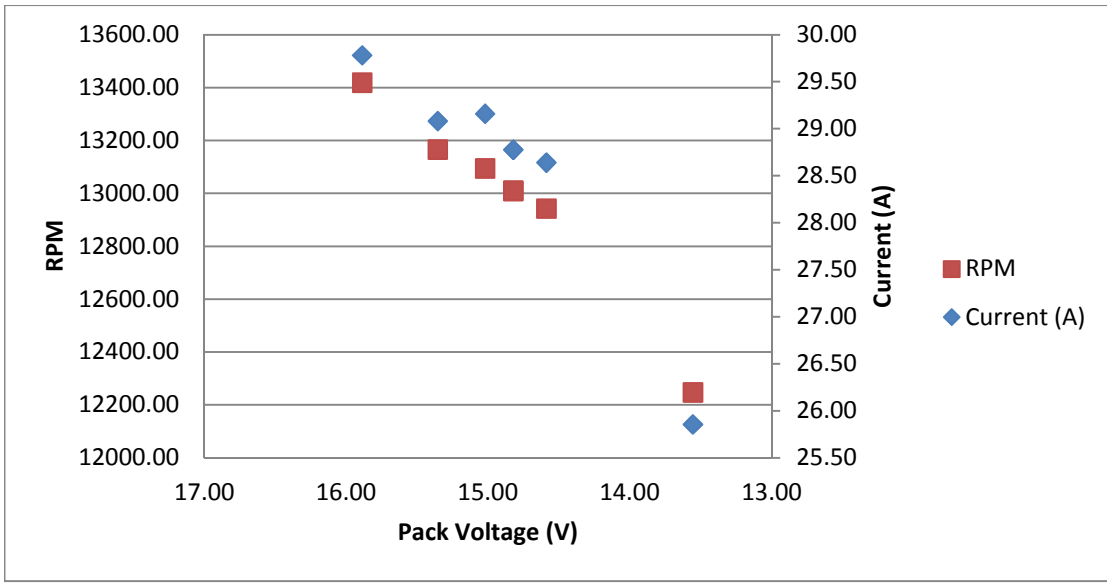

Figure 13 – RPM and Current plotted against battery voltage. Notice that the decreases are proportional, indicative of the very small change in motor efficiency measured in this test.

Because of the limitations of the previous test, the second test procedure was developed to hold three separate voltages at a constant value using the BK Precision XLN3640 DC power supply. With a constant voltage set on the power supply, the output RPM could be adjusted to the same level for each test, resulting in constant output power. With both the input voltage and output power set at approximately constant values, the change in operating efficiency and current draw can be evaluated. Table 7 contains the raw data for the first set of test runs. For these runs, the chosen RPM value was 12,000 RPM. Unfortunately, with the power supply set to 12V the motor was unable to output enough power to reach this RPM value, even at full power.

Table 7 – Constant RPM runs at varying input voltages. N=12000 RPM.

Torque (Lb-in)	Thrust (Lb)	Voltage (V)	Current (A)	RPM	Power in (W)	Power Out (W)	Motor Efficiency (%)
1.87	2.93	16.38	21.18	12079.16	346.88	263.29	75.90
1.91	2.99	14.22	23.97	12122.27	340.94	270.78	79.42
1.64	2.49	11.43	22.00	11127.42	251.52	212.39	84.44

It can immediately be seen that holding a constant voltage and matching the approximate RPM value has produced results that provide a better insight into the actual performance of the system. At approximately the same RPM and thrust output, there is an observed 3.52% increase in efficiency when the voltage setting is dropped to 14.22 V as opposed to 16.8 V. Also interesting to note is the voltage drop through the transmission of power from the power supply to the Eagle Tree logger which is inside the windtunnel attached directly to the motor controller. The voltage settings on the power supply were 16.8, 14.8, and 12 volts respectively, each is showing more than half a volt of losses through the power wires leading from the power supply to the testing apparatus. This does not affect the validity of the results, but if it is desired that the voltage the motor receives is exactly that output by the power supply it would be necessary to use much larger wiring from the power supply to the motor and controller assembly. The current 13 gauge wiring, while able to withstand the current draw, has too high a resistance value at the length needed to reach from the interior of the windtunnel to the power supply.

Figure 14 shows motor efficiency plotted against input voltage. It is important to note when looking at this data that the output power level for the data point at 11.43 V is lower than that for the previous two points, so it is likely higher than the actual value.

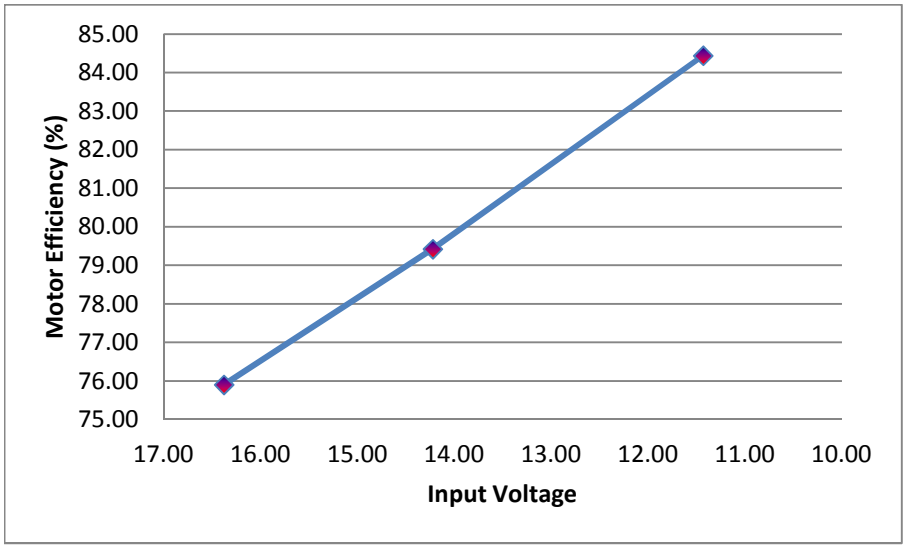

Figure 14 – Motor Efficiency at different input Voltages. Note that the 11.43 V input case was not able to reach the required power level.

Even disregarding the last case, it is obvious from this graph that holding input voltage at constant levels and matching the output power results in much more meaningful values. A 3.52% increase in efficiency is larger than the maximum difference measured in the last test by a factor of 2.8. These results are also interesting as they point to the possibility of the motor and controller having a peak efficiency current draw. It was previously thought that reducing the amperage by increasing the input voltage, at a given power level would increase efficiency. As this

plot shows, not only is this not the case but it is likely that the opposite is true. This would lead to peak performance at a specific amp draw for a given power level. Knowing this, motor and controller systems should be designed to operate as close to this point as possible for the longest period of time. This will result in sizing the motor for the cruise flight requirements.

After looking at efficiency, it is informative to look at the power in and power out values directly. These are shown in Figure 15.

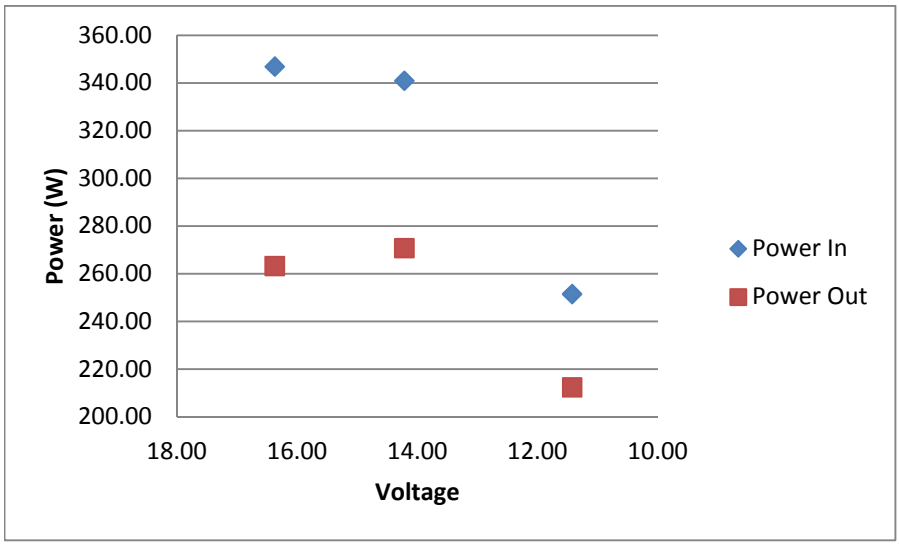

Figure 15 – Power In and Power Out for varied input voltages.

As before, the third data point is tainted by the system's inability to reach 12000 RPM at the chosen input voltage (12V). That said, the first two data points are of interest. Note that there is a slight increase in output power and a slight decrease in input power for the set of data points corresponding to the 14.8V power supply setting. This is reflected by the increase in efficiency reported earlier. The closer these two values are to one another the higher the efficiency reached by the motor. With enough data points, this relationship could be used to graphically choose the best input voltage for a given motor, propeller, and power output combination.

The last parameters to analyze from this data set are RPM and motor current. This data is plotted in Figure 16. Of note is the reversal in trends from that shown in Figure 11. At the lower input voltage of 14.8 V the current draw is greater than that at 16.8 V. This is because for a given output power at a lower voltage more current is needed to make up for the loss in input voltage. The last datapoint on this graph, although of limited importance because the power output is not matched, is interesting in this case because it shows that when the power level desired is higher than what the motor is capable of with a specific propeller and input voltage combination, the current draw can actually be higher than it would be at a higher input voltage. The last data point on this graph was run at 100% power. While efficiency is high, this higher amp draw will result in faster discharge times at this power level than a higher voltage setup would exhibit, assuming the same battery cells are used but in a different series configuration (more or fewer cells in series).

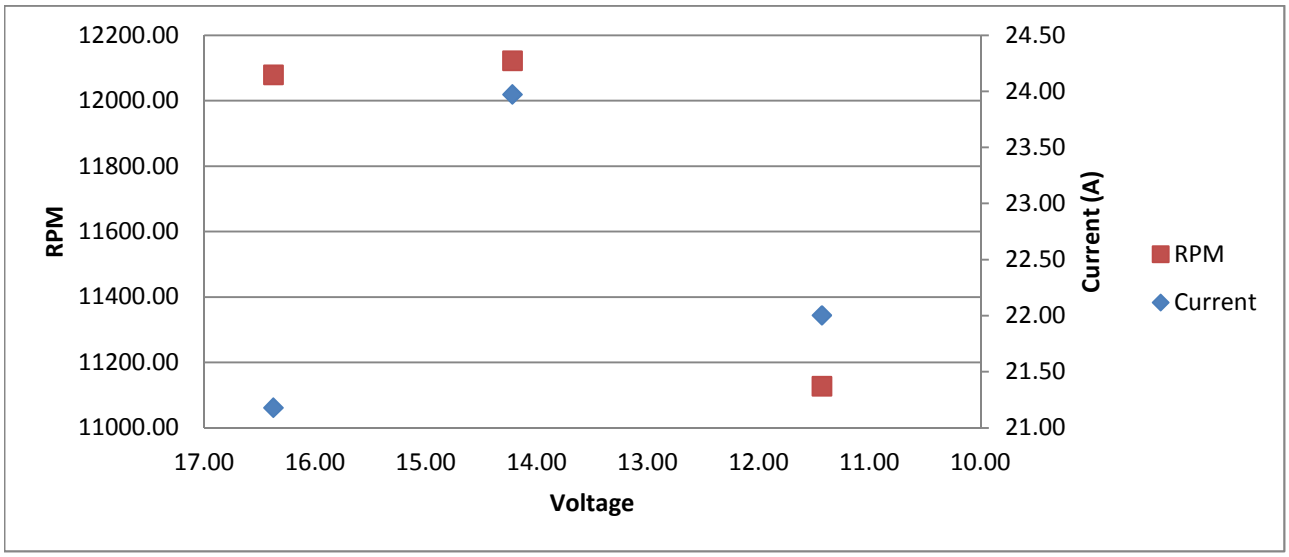

Figure 16 – Motor RPM and Current for varied input voltages

Because the RPM selected for the previous test was outside of the system's capability at 12 V input, a second set of tests was performed to provide a full set of data with which to analyze the effects of input voltage on motor efficiency. This data is seen in Table 8.

Table 8 – Measurements taken at varying input voltages at N=10,000 RPM.

Torque (Lb-in)	Thrust (Lb)	Voltage (V)	Current (A)	RPM	Power in (W)	Power Out (W)	Motor Efficiency (%)
1.27	1.99	16.43	12.81	9941.73	210.40	147.86	70.28
1.31	2.03	14.34	14.38	10152.56	206.15	155.09	75.23
1.29	2.01	11.43	16.24	10080.48	185.70	151.47	81.57

These results further support the evidence from the last test that motor efficiency is tied more directly to amp draw than to voltage. Again improvements in motor efficiency are seen as the current draw increases. The maximum output potential of the motor is more limited at lower voltages, but if the necessary performance can be had at a lower voltage it may be advantageous to run fewer, larger cells in series to allow the motor to operate in its peak efficiency current range. Figure 15 shows the relationship between input voltage and motor efficiency at this operating point. The inversely proportional relationship between motor efficiency and input voltage is clear to see. It is likely that this effect is due to the difference in duty cycle used by the controller at different input voltages at the same power level. Electric motor controllers use pulse width modulation to regulate the output power of the motor. With a higher input voltage, the duty cycle, or the amount of time the controller spends in the "on" position is shorter. It is likely that this has a negative effect on the efficiency of the system. Because of this, designers of electric power systems should be careful of oversizing the power system for the intended application. Not only does this add weight, but cruising at too low a throttle setting can negatively affect the overall motor efficiency. It may be worthwhile to require a bungee or other assisted launch system rather than a simple hand launch to facilitate use of a smaller drive system if maximum flight time is going to be achieved. The benefits of a system like this may be limited by the need to operate under adverse flight conditions, excess power may be necessary for flight in inclement weather or even strong winds if the system is to be usable under any weather conditions.

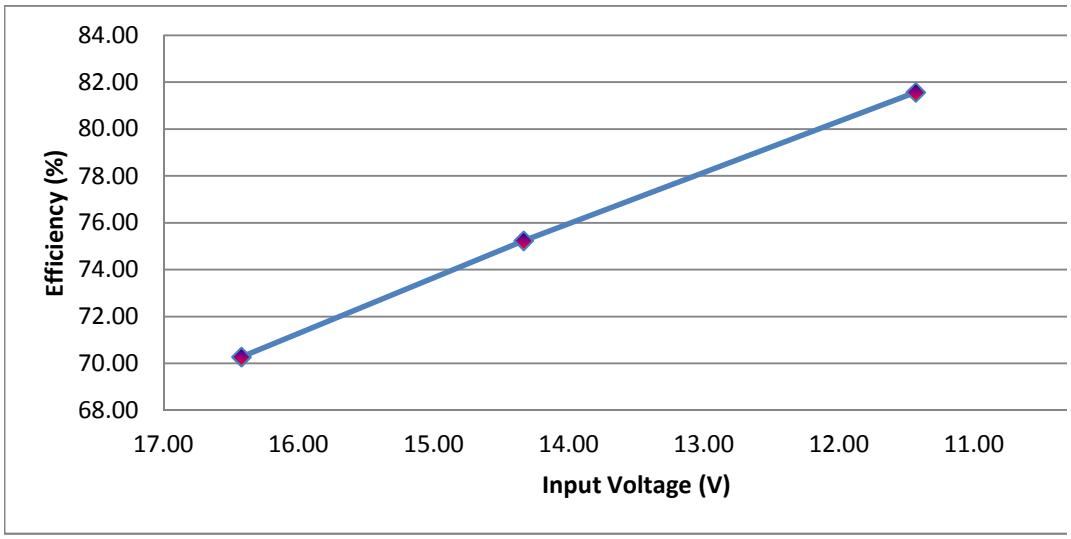

Figure 17 – Motor Efficiency plotted against input voltage at N=10,000 RPM.

As in the previous data set, the next metric to consider is the relationship between power in and power out. This is shown in Figure 18.

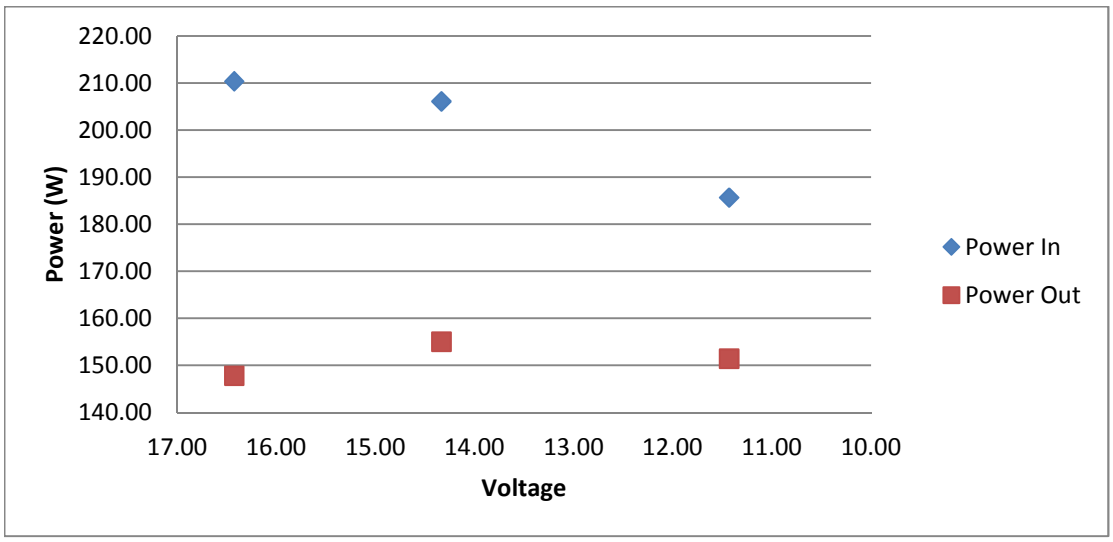

Figure 18 – Power in and power out plotted against input voltage at N=10,000 RPM. Note the continuance of the trend observed in the last test with a smaller difference in input and output power as input voltage is decreased.

Again it is shown that performance is higher when the input voltage is lower as evidenced by the reduced distance between the power in and power out curves as the input voltage is dropped. Figure 19 shows the RPM and current values for this test run.

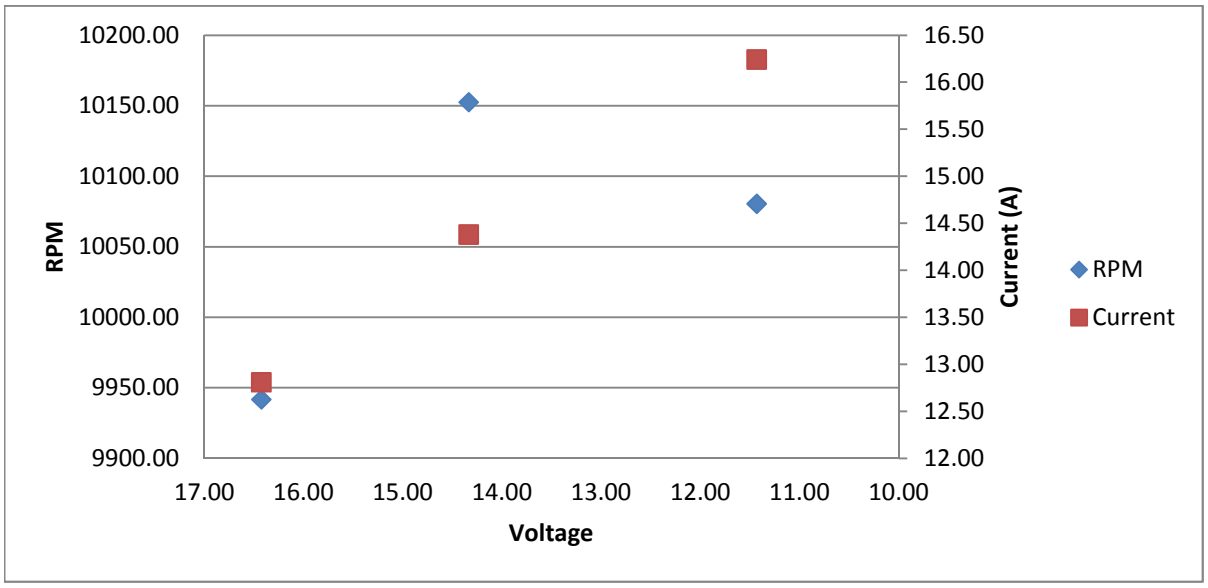

Figure 19 – RPM and current for N=10,000 RPM test case. Notice that actual RPM values are very close to the desired 10,000 rpm.

With these tests completed, the tests to determine the combined performance of the motor and propeller under simulated flight conditions could begin. This data is tabulated in the appendix as it is too large to insert directly into the text. When looking at this data, there are two issues that cause problems with the validity of the data. First, under some conditions the measured torque is extremely small. Due to the nature of the calibration method used and the fact that the calibration equation has a negative offset some of these extremely small torque values record as negative values. These data points are not useable for any meaningful calculation. Likewise, under some combinations of throttle input and tunnel velocity the prop is not generating enough pitch speed to produce any thrust and in fact is causing drag. As the setup of the swivel clevis prevents accurate axial compression measurements the system cannot accurately measure this drag, and again these data points are meaningless. To analyze this data, it is important to look at it from two perspectives. Both the power setting and flight velocity have an effect on the performance of the propeller. Because of this, propeller performance will be plotted against both of these metrics.

First, motor performance for each run condition is compared. Figure 20 displays the overlaid motor efficiency data for each run condition. From this graph it can be seen that flight condition has relatively little effect on the performance of the motor and controller system. The largest variance is observed at 40% throttle, where for the higher velocity cases propeller unloading has a large effect on the load applied to the motor. Once the propeller is generating thrust and the amp draws at each power setting come more into alignment for each commanded throttle input the variation in motor efficiency between test runs was relatively small, usually around 2-3% given the same throttle input.

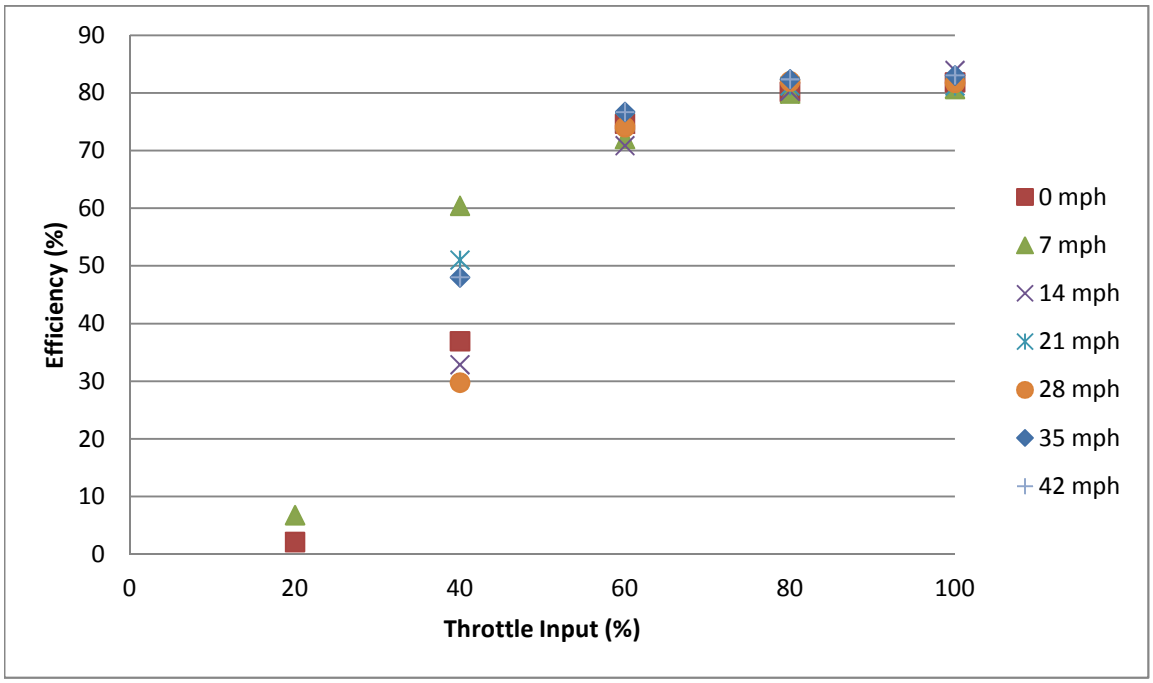

Figure 20 – Motor Efficiency for each run flight velocity plotted vs. commanded throttle input.

With the motor efficiency parameters matching up well with what was expected, the propeller parameters can be analyzed. Figure 21 shows propeller efficiency plotted against tunnel velocity for each commanded power input. This data shows the limitations of the measurement system. The 20% and 40% throttle data is highly erratic, with both cases having unbelievably high peak efficiencies for the 28 mph case. It is highly likely that these values are caused by the very small scale of the torque and thrust values produced by these power settings under any substantial flight velocity. If accurate propeller characteristics for these two power levels are desired it would be necessary to run more tests at a much lower wind tunnel freestream velocity, otherwise the magnitude of the measurements is just too small to measure accurately.

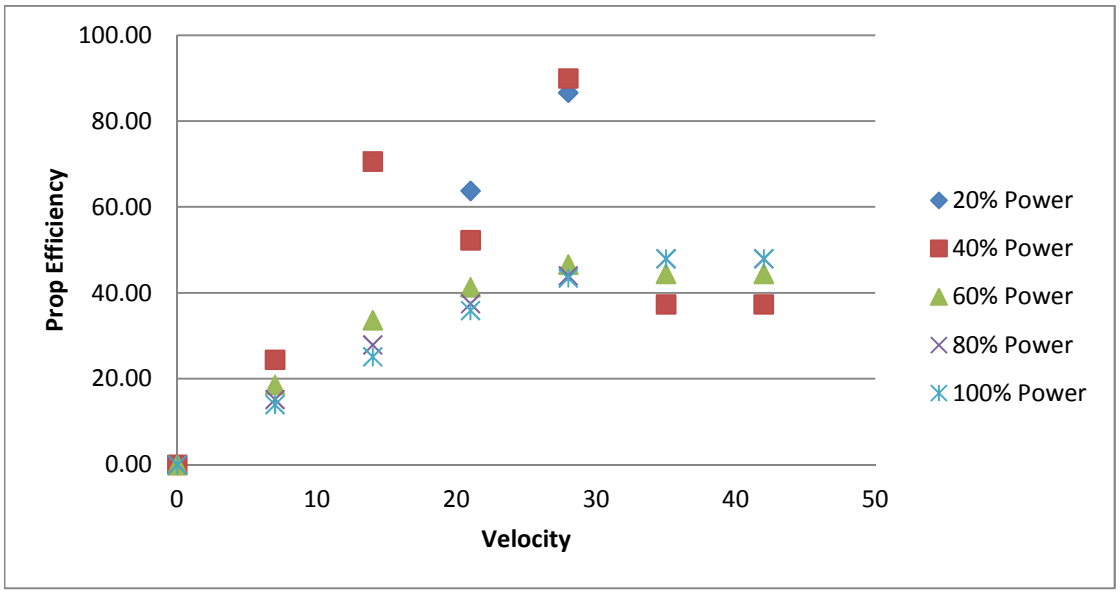

Figure 21 – Propeller efficiency curves for each commanded power setting

Unlike the 20% and 40% power cases, the 60% and up cases show very good trending towards an efficiency plateau of around 50% in each case. Interestingly, peak efficiency does not vary much between these three cases. Judging by this graph, the APC E 9x4.5 has more pitch speed to spare at 42 mp and 100% throttle with this setup. Further testing would be necessary to find out when the pitch speed and therefore propulsive efficiency would drop off above this point.

An interesting trend that can be observed in the propeller and motor efficiency data is that the general trends for this data are exactly opposite that which is optimal. This is shown in Fig. 22. The efficiency of the propeller, in general, decreases as the motor efficiency increases. In this configuration, there is no at which the system as a whole is optimized. At any operating condition, the motor, propeller, or both will be off of their maximum efficiency point, resulting in poor efficiency across the board. To minimize total energy usage, a motor and propeller combination should be setup such that as much as possible the efficiency peaks overlap near the cruise condition where the aircraft is going to spend the largest percentage of its time. Interestingly, this trend is not seen to the same degree in the 35 and 42 mph cases. This is likely due to the changes in propeller efficiency due to unloading.

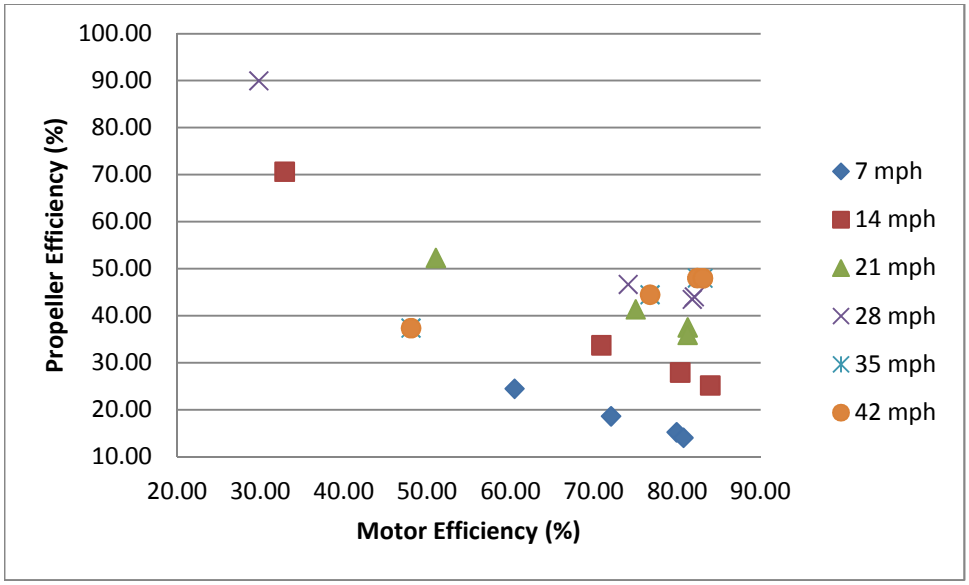

Figure 22 – Motor and Controller efficiencies do not synchronize in an effective manner.

VI. Error Analysis

As one of the goals of this experiment was to determine whether this system is able to accurately characterize the properties of a motor and propeller drive system performing error calculations is an important part of validating any data taken using this apparatus. The error analysis shown in this section was completed using the data from the 28 mph, 60% throttle case.

Table 9 lists the standard deviation data for each of the measurements taken by this apparatus.

Table 9 – Standard Deviation of data for 28 mph, 60% throttle run condition.

Measurement	StDev (Absolute)	StDev (%)
rpm	±230.9712	2.39
Thrust (lb)	±0.319474	29.74
Torque (lb-in)	±0.222862	19.56
Amps	±0.034519	*2.87*
Volts	±0.006794	$4.7x10^{-4}$

From looking at this data, it appears that the Eagle Tree data logger is a relatively accurate device, with voltage and amperage standard deviations measuring in the thousandths and hundredths respectively. Unfortunately, the standard deviation on the torque and thrust values is a bit higher than optimal, at approximately 7% and 15% of an average reading for those two measurements and 19.56% and 29.73% of the values actually recorded for the data point used. Part of this is likely due to noise in the measurement system and the stiction problems mentioned earlier in the report, but also these standard deviations are including any oscillations or variations in the actual system. There was an observed resonance in the motor and propeller system for the 60% and 80% throttle cases which was not present in the 20%, 40%, or 100% throttle runs at any airspeed. These oscillations visibly increased the size of the standard deviation on the LabView data acquisition panel from the standard deviation observed when taking the calibration measurements. Using the 2 lb thrust calibration data, the standard deviation is 2.33x10^-14, which leads me to believe that these high values are in part a problem of the actual drive system's ability to maintain a perfectly constant thrust and torque output and not a problem with the measurement system itself. With that said, it is important to know how these measurement variations affect the calculated parameters. To judge the accuracy of the measurements found by this apparatus, the motor power out standard deviation will be used as a parameter which should provide similar results to those calculated for the other parameters found in this report.

The standard deviation of a calculated value made up of the product of two values (from Eq. 15 power is calculated from the product of RPM and torque) is made up of the effects of the deviations of each variable that goes into that value. This is represented by the function shown in Eq. 8.[8]

$$\left(\frac{\delta P}{P}\right)^2 = \left(\frac{\delta RPM}{RPM}\right)^2 + \left(\frac{\delta T}{T}\right)^2 \tag{22}$$

Where A and B are the values being multiplied and Z is the final value of the product. Rearranging for ΔZ, this equation becomes

$$\delta P = P\sqrt{\left(\frac{\delta RPM}{RPM}\right)^2 + \left(\frac{\delta T}{T}\right)^2}$$

Performing this calculation for the 60% throttle, 28 mph case

$$\delta P = 128.2210675\sqrt{\left(\frac{230.9712}{9642.7009}\right)^2 + \left(\frac{0.222862}{1.139444}\right)^2} \tag{23}$$

Which results in a δP value of 25.27 W. This constitutes a $\pm 20\%$ margin of error, which is clearly larger than acceptable considering percentage changes in motor efficiency of less than 10% are significant. If the values in this report are to be believed, it is absolutely necessary to believe that this deviation is a result of oscillations in the actual system being tested and that the average value is the true mean value being recorded. If the standard deviation is not being affected by the variation in the test power system then the apparatus is highly susceptible to error and requires substantial work to make it perform to an acceptable level.

VII. Recommendations for Future Research and Improvement

Before performing any future research, more work should be put into analyzing the accuracy and precision of the system. As measured, I would not be willing to stake the performance of an aircraft destined for combat operations on the measurements provided by this system. Both the torque and thrust measurements are in need of significant need of improvement.

One of the problems that was immediately apparent when using the system was stiction in the bearing system and in the linkages separating the torque and thrust measurement systems. To improve this, flexures could be used in place of the complicated bearing swivel and heim joint portion of the apparatus. Flexures provide nearly stiction free movement over a small range of motion, which is all that is required by the apparatus as the torque and thrust measurements do not allow for the apparatus to move to any great degree to begin with. Finding a way to link these two measurement systems while reducing the mass of the components as well as their stiction is an important next step. If flexures are found to be impractical, experimentation should be done with different lubricants to minimize the amount of friction in the system. The tests in this report were done using a simple turbine oil as the lubricant for all joints and the linear bearing system. This lubricant does not have the low resistance properties of a graphite or Teflon type lubricant, and now that it has been determined that stiction is a serious issue this should be addressed.

Another improvement that would prove worthwhile is development of an integrated system which has the ability to measure all necessary data through one computer program. While using two programs to record data resulted in usable data, it was an added level of complexity and made live observation of all data being recorded difficult.

Once these issues are taken care of, testing of various propeller and motor combinations is the logical next step. As shown in this report, choosing a propeller that best matches the power system has a very large effect on the system efficiency. If the propeller and motor are improperly matched from an efficiency standpoint, the entire range of operation will be at low efficiency due to one component or the other.

VIII. Conclusion

In conclusion, it was found that the system provided reasonable data for a large majority of operating conditions. Under windtunnel test conditions it was able to determine propeller and motor efficiencies consistently for three out of five power levels and for all freestream velocities. It was determined that for the motor and propeller combination used in this test, the motor was not properly matched to the propeller if efficiency optimization is the main goal of the design. From a design improvement perspective, the system pointed to the propeller being the most likely source of efficiency improvement with propeller measuring across the board much higher than those of the motor itself.

One significant and unexpected result was the determination that motor efficiency is highly dependent on input voltage but with the opposite correlation to the expected outcome-a higher than necessary input voltage forces the motor controller to operate at a lower duty cycle for a given power output which reduces system efficiency. If maximum cruise efficiency for a system designed for extended loiter times is to be achieved, care should be taken to prevent oversizing the motor and controller system. Oversizing the motor and controller will result in lower cruise efficiencies, and as such the motor and controller system should be selected so that the excess power is just enough for emergency maneuvers or to overcome weather conditions.

Unfortunately, the test system proved to have a high level of standard deviation, with a calculated sample error on the motor shaft power measurement of 20%. This high amount of error is much too high to allow for any significant conclusions about the results to be made without some explanation as to why the standard error measurements are so high. Until this value is reduced, the effectiveness of this apparatus as a tool for the evaluation of real UAV power systems is limited at best. It is likely that this variation is due to oscillations in the output torque and thrust of the motor and propeller system, but until this is verified the results cannot be accepted at face value.

Future research should focus on improving the apparatus, after which point the system could be used to find a more optimal propeller setup for this motor and controller combination. Finding a motor and propeller combination that works together at peak efficiency will result in a system with much higher average efficiency and thus longer flight times.

Appendix

1. Raw Averaged Data For Windtunnel Tests.

Throttle (%)	Torque (Lb-in)	Thrust (Lb)	Voltage (V)	Current (A)	RPM	Power in (W)	Motor Power Out (W)	Motor Efficiency	Prop Power Out (W)	Propeller η (%)
V=0										
20.00	0.01	0.21	14.81	1.61	4004.62	23.84	0.51	2.13	0.00	0.00
40.00	0.41	1.02	14.60	6.53	7442.43	95.43	35.27	36.96	0.00	0.00
60.00	1.24	1.89	14.33	13.33	9854.64	191.01	142.64	74.68	0.00	0.00
80.00	1.77	2.69	13.98	21.31	11600.26	297.95	238.97	80.20	0.00	0.00
100.00	2.19	3.36	13.61	29.37	12812.31	399.74	327.17	81.85	0.00	0.00
V=7 mph										
20.00	0.04	0.14	14.79	1.78	4349.98	26.38	1.79	6.79	1.98	110.38
40.00	0.68	1.06	14.59	6.86	7575.36	100.11	60.52	60.45	14.80	24.46
60.00	1.17	1.74	14.40	12.52	9538.52	180.21	129.80	72.03	24.15	18.61
80.00	1.80	2.68	14.07	21.85	11696.28	307.37	245.59	79.90	37.34	15.20
100.00	2.20	3.35	13.77	29.95	12944.07	412.46	332.90	80.71	46.66	14.02
V=14 mph										
20.00	-0.04	0.20	14.82	1.56	4379.72	23.08	-2.16	-9.37	5.67	-262.09
40.00	0.37	0.82	14.64	6.74	7471.70	98.62	32.43	32.88	22.90	70.63
60.00	1.16	1.55	14.42	12.54	9474.91	180.82	128.14	70.86	43.17	33.69
80.00	1.82	2.49	14.07	21.98	11669.41	309.26	248.38	80.32	69.35	27.92
100.00	2.32	3.16	13.78	30.25	12927.32	417.02	349.96	83.92	88.03	25.16
V=21 mph										
20.00	0.10	0.09	14.82	1.58	4906.38	23.45	5.89	25.12	3.76	63.79
40.00	0.54	0.61	14.64	6.48	7699.20	94.87	48.41	51.02	25.31	52.28
60.00	1.27	1.43	14.39	13.38	9755.85	192.60	144.42	74.98	59.74	41.37
80.00	1.84	2.23	14.08	21.71	11564.34	305.75	248.34	81.22	93.19	37.52
100.00	2.26	2.92	13.78	30.38	12914.50	418.74	340.04	81.21	122.11	35.91
V=28 mph										
20.00	-0.06	-0.06	14.82	1.52	5459.75	22.60	-3.98	-17.60	-3.45	86.66
40.00	0.29	0.44	14.65	6.17	8033.60	90.47	26.94	29.78	24.24	89.96
60.00	1.14	1.07	14.44	11.99	9642.70	173.08	128.22	74.08	59.81	46.64
80.00	1.83	1.95	14.11	21.27	11546.86	300.04	246.08	82.01	108.30	44.01
100.00	2.27	2.67	13.78	30.33	12924.06	418.14	341.92	81.77	148.64	43.47
V=35 mph										
20.00	-0.02	-0.12	14.81	1.40	6163.23	20.76	-1.13	-5.44	-8.07	714.84
40.00	0.41	0.21	14.63	5.60	8302.75	81.93	39.35	48.03	14.70	37.35
60.00	1.09	0.81	14.39	11.45	9893.78	164.72	126.34	76.70	56.17	44.46
80.00	1.73	1.60	14.02	20.12	11493.55	282.00	232.29	82.37	111.52	48.01
100.00	2.22	2.30	13.64	29.43	12871.18	401.49	333.44	83.05	159.94	47.97
V=42										

mph

20.00	0.03	-0.39	14.81	1.30	7021.96	19.30	2.24	11.60	-32.87	-1468.44
40.00	0.41	0.21	14.63	5.60	8302.75	81.93	39.35	48.03	14.70	37.35
60.00	1.09	0.81	14.39	11.45	9893.78	164.72	126.34	76.70	56.17	44.46
80.00	1.73	1.60	14.02	20.12	11493.55	282.00	232.29	82.37	111.52	48.01
100.00	2.22	2.30	13.64	29.43	12871.18	401.49	333.44	83.05	159.94	47.97

Acknowledgments

The author would like to thank Dr. John Dunning and Dr. Thomas Mackin for their support and input as advisors.

The author would also like to thank Jarred Pinn and Joshua Roepke for their support in prepping the windtunnel for use by this project.

The author would like to thank the CREATT Project and the Department of Energy for funding this research.

The author would last like to thank Cody Thompson and Precision Machine for their assistance in building the testing apparatus.

References

[1]Barlow, Jewel B., Rae, William H., and Pope, Alan, *Low Speed Windtunnel Testing*, Wiley, New Jersey, 1999, pp. 218-220.

[2]Bourassa, James, Rosz, John, "Calculating Horsepower, RPM, and Torque," WISC-Online, 2004. [http://www.wisc-online.com/Objects/ViewObject.aspx?ID=ENG17504. Accessed 12/6/11.]

[3]Coba, Javier V., "Application Of Copper Indium Gallium Diselenide Photovoltaic Cells to Extend the Endurance and Capabilities of the Raven RQ-11B Unmanned Aerial Vehicle," Naval Postgraduate School, 2010.

[4]Halliday, David, Resnick, Robert, Walker, Jearl, *Fundamentals of Physics,* Wiley, New Jersey, 2007, pp. 200.

[5]Dr. Jin Tso, California Polytechnic State University San Luis Obispo Aerospace Engineering Department, Personal Correspondence, July 2011.

[6]Rother, Peter, "Why does the Torquemax Rotate so Slowly and So Forcefully," Torquemax, The LRK Site, [http://www.aerodesign.de/peter/2001/LRK350/Warum_dreht_er_so_eng.html. Accessed 10/31/11.]

[7]Rother, Peter, "Torquemax, Who will not Build It?" Torquemax, The LRK Site, [http://www.aerodesign.de/peter/2001/LRK350/LRK350-20-15_eng.html. Accessed 10/31/11.]

[8]Taylor, John R., *An Introduction to Error Analysis: The Study of Uncertainties of Physical Measurements*, University Science Books, California, 1982, pp. 61.

[9]Unknown, "AVX-50BL10 50V, 10A Brush / Brushless Power Amplifier Data Sheet and Setup Guide," Aveox, Inc.

[10]Unknown, "Analog to Digital Conversion," Measurement Computing, [http://www.mccdaq.com/PDFs/specs/Analog-to-Digital.pdf. Accessed 12/4/11.]

[11]Unknown, "Bus-Powered M Series Multifunction DAQ for USB - 16-Bit, up to 400 kS/s, up to 32 Analog Inputs, Isolation," National Instruments, [http://sine.ni.com/ds/app/doc/p/id/ds-9/lang/en. Accessed 12/6/11.]